Title

Ultrashort echo time MRI detects significantly lower collagen but higher pore water in the tibial cortex of female patients with osteopenia and osteoporosis

Journal

Journal of Bone and Mineral Research, 39(6)

ISSN

0884-0431

Authors

Jerban, Saeed

Ma, Yajun

Wei, Zhao

et al.

Publication Date

2024-07-23

DOI

10.1093/jbmr/zjae053

Peer reviewed

Journal of Bone and Mineral Research, 2024, **39**, 707–716
https://doi.org/10.1093/jbmr/zjae053
Advance access publication: April 9, 2024
Research Article

Ultrashort echo time MRI detects significantly lower collagen but higher pore water in the tibial cortex of female patients with osteopenia and osteoporosis

Saeed Jerban[1,*], Yajun Ma[1], Zhao Wei[1], Meghan Shen[1], Zubaid Ibrahim[1], Hyungseok Jang[1], Pengzhe Lu[2,3], Douglas G. Chang[4], Gina Woods[5], Christine B. Chung[1,2], Eric Y. Chang[1,2], Jiang Du[1,2,*]

[1]Department of Radiology, University of California, San Diego, CA 92093, United States
[2]Research Service, VA San Diego Healthcare System, San Diego, CA 92161, United States
[3]Department of Neurosciences, University of California, San Diego, CA 92093, United States
[4]Department of Orthopaedic Surgery, University of California, San Diego, CA 92093, United States
[5]Department of Medicine, University of California, San Diego, CA 92093, United States

*Corresponding authors: Jiang Du, Department of Radiology, University of California, San Diego, 9500 Gilman Dr., La Jolla, CA 92093, United States (jiangdu@health.ucsd.edu); Saeed Jerban, Department of Radiology, University of California, San Diego, 9500 Gilman Dr., La Jolla, CA 92093, United States (sjerban@health.ucsd.edu).

Abstract

Ultrashort echo time (UTE) MRI can quantify the major proton pool densities in cortical bone, including total (TWPD), bound (BWPD), and pore water (PWPD) proton densities, as well as the macromolecular proton density (MMPD), associated with the collagen content, which is calculated using macromolecular fraction (MMF) from UTE magnetization transfer (UTE-MT) modeling. This study aimed to investigate the differences in water and collagen contents in tibial cortical bone, between female osteopenia (OPe) patients, osteoporosis (OPo) patients, and young participants (Young). Being postmenopausal and above 55 yr old were the inclusion criteria for OPe and OPo groups. The tibial shaft of 14 OPe (72.5 ± 6.8 yr old), 31 OPo (72.0 ± 6.4 yr old), and 31 young subjects (28.0 ± 6.1 yr old) were scanned using a knee coil on a clinical 3T scanner. Basic UTE, inversion recovery UTE, and UTE-MT sequences were performed. Investigated biomarkers were compared between groups using Kruskal–Wallis test. Spearman's correlation coefficients were calculated between the TH DXA T-score and UTE-MRI results. MMF, BWPD, and MMPD were significantly lower in OPo patients than in the young group, whereas T1, TWPD, and PWPD were significantly higher in OPo patients. The largest OPo/Young average percentage differences were found in MMF (41.9%), PWPD (103.5%), and MMPD (64.0%). PWPD was significantly higher (50.7%), while BWPD was significantly lower (16.4%) in OPe than the Young group on average. MMF was found to be significantly lower (27%) in OPo patients compared with OPe group. T1, MMF, TWPD, PWPD, and MMPD values significantly correlated with the TH DXA T-scores (provided by the patients and only available for OPe and OPo patients). DXA T-score showed the highest correlations with PWPD (R = 0.55) and MMF (R = 0.56) values. TWPD, PWPD, and MMF estimated using the UTE-MRI sequences were recommended to evaluate individuals with OPe and OPo.

Keywords: MRI, cortical bone, ultrashort echo time, pore water, magnetization transfer, collagen proton density

Lay Summary

Ultrashort echo time (UTE) is an MRI technique that can quantify the water and collagen content of cortical bone. Water in the bone can be found residing in pores (pore water) or bound to the bone matrix (bound water). We investigated the differences in water and collagen contents of tibial cortical bone between female osteopenia patients, osteoporosis patients, and young participants. Bound water and collagen contents were significantly lower in osteoporosis patients than in the young group, whereas total water and pore water contents were significantly higher in osteoporosis patients. Pore water was significantly higher, while bound water was significantly lower in osteopenia than in the Young group. Collagen content was found to be significantly lower in osteoporosis patients compared with the osteopenia group. The estimated water and collagen contents were significantly correlated with the TH bone densitometry measures in the patients.

Introduction

The World Health Organization regards areal BMD assessment using DXA as the gold standard for osteoporosis (OPo) diagnosis in the over 50-yr-old population in several racial and ethnic groups.[1–6] It is important to note that bone composition is not limited to only the mineral component, but is also comprised of the organic matrix, water, and fat, which together represent the major portion of the bone volume (>90% in trabecular bone sites and > 55% in cortical bone sites).[7] These latter components contribute significantly to the mechanical properties of bone,[8,9] but cannot be rigorously evaluated by DXA or other X-ray-based techniques.[10]

Quantitative bone evaluation using MRI has recently received more attention as a method that can evaluate the bone's organic matrix and water content while avoiding the potential harm associated with ionizing radiation.[11-25] Aside

Received: July 15, 2023. **Revised:** March 10, 2024. **Accepted:** April 4, 2024

from these safety concerns, MRI-based bone assessment also allows the evaluation of surrounding soft tissues, such as the ligaments, tendons, and muscles.[26,27] Although clinical MR sequences can be utilized for morphological assessment, they are not capable of quantitative bone evaluation due to the negligible signals.[19-21] In more details, the magnitude of the acquired MR signal in bone is a function of its apparent spin–spin relaxation time (T2*), which is very short (ie, on the order of hundreds of microseconds)[11,12] and cannot be detected by clinical sequences utilizing echo times (TEs) of several milliseconds. Alternatively, ultrashort echo time (UTE) sequences with TEs under 0.05 ms are able to acquire MR signals from bone.[19-21]

Hydrogen protons in macromolecules, bound water, and pore water are the 3 major proton pools in cortical bone.[12] Total water proton density (TWPD) and bound water proton density (BWPD) can be measured by comparing a reference signal (usually from an external reference with a known proton density, for example, 20% H_2O and 80% D_2O) with the bone signals in UTE-MRI and inversion recovery UTE-MRI sequences, respectively.[12,28] Pore water proton density (PWPD) can be estimated by subtracting BWPD from TWPD. UTE magnetization transfer (UTE-MT) imaging can be used to indirectly measure the macromolecular proton fraction (MMF) in cortical bone based on 2-pool (water vs macromolecules) MT modeling,[29,30] allowing macromolecular proton density (MMPD) to be then estimated as a function of MMF and TWPD.

Earlier ex vivo investigations on human cortical bone have demonstrated that bone porosity, BMD, and mechanical properties significantly correlate with TWPD, PWPD, and MMF.[20,21,31-33] The feasibility of in vivo assessment of TWPD, BWPD, PWPD, MMF, and MMPD was investigated in a prior study where elderly participants demonstrated higher TWPD and PWPD values, while lower MMF, BWPD, and MMPD values compared with young participants.[32]

This study aimed to investigate the differences in water proton densities (TWPD, BWPD, and PWPD) and macromolecular proton densities (MMF and MMPD) between postmenopausal osteopenia (OPe) patients, OPo patients, and young female participants.

Materials and methods

Subject inclusion

A total of 82 female participants were recruited for MRI scans: 31 young subjects and 51 post-menopausal participants with recent (<2 mo) hip DXA scans. Participants were recruited using flyers in Radiology, Orthopedics, and Endocrinology clinics at UCSD. To be included in the young group, individuals must (1) be under 45 yr old and pre-menopausal and (2) not be pregnant (urine test was performed before MRI scan). To be included in the post-menopausal groups, individuals must (1) be above 55 yr old and post-menopausal and (2) provide a recent (past 2 mo) hip DXA scan report. All the individuals must be willing and able to complete a 1–h MRI in the supine position. Individuals with trauma and significant leg and hip injuries within the past 12 mo were excluded. Of the postmenopausal participants, 6 were normal (Total Hip (TH) DXA T-scores > −1), 14 were OPe patients (T-scores between −2.5 and −1), and 31 were OPo patients (DXA T-scores below −2.5). DXA reports were not available for young participants. Normal postmenopausal participants were excluded from the study due to their limited number, which might challenge further comparisons between groups. It should be noted that the non-ethnically matched DXA scores generated in multiple clinical facilities were submitted by the patients and recorded by the study coordinator. The Ope and Opo status was determined based on the TH DXA scores, which were available for all the recruited postmenopausal patients and could be trusted regardless of the potential differences in the methods and scanners. Menopausal status was determined by the patient's report. Current medical treatment and fracture history were not investigated in this study.

This study was approved by the institutional review board of the University of California, San Diego. Written informed consent was obtained from each participant. This research study was conducted compliant with the applicable good clinical practice requirements and the relevant guidelines and regulations.

UTE-MR imaging

All participants were scanned on a 3 Tesla clinical MRI scanner (MR750, GE Healthcare Technologies) using an 8-channel knee coil (transmit and receive coil). Young participants were asked to choose on their own which leg should be scanned in MRI, regardless of their leg dominance. For post-menopausal patients, the leg selection had to match the available side in the hip DXA scan reports. The MR imaging coverage was centered in the middle of the tibial shaft, according to the operator's experience. TWPD, BWPD, and PWPD estimation in tibial cortical bone were performed via MR signal comparison between bone and an external reference of known proton density (22 mol/L H1 composed of 20% volume H_2O and 80% volume D_2O, doped with 24 mmol/L $MnCl_2$, $T2 \approx 0.35$ ms, $T1 \approx 6$ ms). The required equations to calculate the estimated proton densities are presented in Appendix I.[12,28]

The 3D UTE, IR-UTE, and UTE-MT sequences were previously described in detail.[12,20,21,29,34] The basic 3D UTE sequence utilized a short rectangular excitation pulse followed by Cones trajectory sampling to acquire signals from both pore and bound water in cortical bone.[12,20] The 3D IR-UTE sequence utilized an 8.64 ms long adiabatic inversion pulse to invert and null pore water magnetization, followed by UTE acquisition to detect signals from bound water.[12,20]

The imaging protocol to estimate the water proton densities included, first, a PD-weighted 3D UTE sequence (repetition time (TR) = 50 ms, TE = 0.032 ms, FA = 10°) for TWPD measurement with a scan time of 3 min, and second, a 3D IR-UTE sequence (TR = 100 ms, TI = 45 ms, TE = 0.032 ms, FA = 20°) for BWPD measurement with a scan time of 3.5 min. A $T_{1\text{-BW}}$ of 135 ms was used for BWPD measurement [Appendix I, eqn. (A4)], as had been previously measured for 8 volunteers.[35] PWPD was calculated by subtracting BWPD from TWPD.

The 3D UTE-MT sequence employed a Fermi pulse (duration of 8 ms) for off-resonance saturation of macromolecular magnetization, followed by UTE acquisition to detect signal from bone water.[29,34] As a prerequisite for UTE-MT modeling and MMF assessment, T1 measurement was performed using a UTE-based actual flip angle imaging-variable TR (UTE-AFI-VTR) sequence (AFI: TE = 0.032 ms, TRs = 20 ms, and 100 ms, VTR: TE = 0.032 ms, TRs = 30, 80, 150 ms, FA = 45°) with a total scan time of 20 min.[36]

T_1 was calculated using a single-component exponential fitting ($S(TR) \propto 1 - \exp(-TR/T1) + constant$) of the acquired data.[36] Fifteen UTE-MT sequences (TE = 0.032 ms, TR = 100 ms, FA = 7°) were performed, providing 3 different saturation power levels (500°, 1000°, and 1500°) and 5 frequency offsets (2, 5, 10, 20, and 50 kHz) for UTE-MT modeling with a total scan time of 13 min. Performing the 2-pool UTE-MT modeling, the MMF biomarker was calculated, an index quantifying the ratio between the collagen and water proton pools.[29,30,34] A Gaussian function was used to model the spectrum of the macromolecular proton pool and its loss of longitudinal magnetization.[29] MMPD was then calculated as a function of TWPD and MMF, obtained from UTE-MT modeling [Appendix I, eqn. (A6)].

The fitting models described above were also used to generate pixel maps of the TWPD, BWPD, PWPD, MMF, and MMPD for presentational purposes in this investigation.

The matrix dimension, field of view (FOV), nominal in-plane pixel size, and slice thickness were $160 \times 160 \times 24$, $140 \times 140 \times 120$ mm^3, 0.87 mm, and 5 mm, respectively. After each human subject scan, the UTE-MRI sequence was used to image a large homogenous water phantom to generate the coil sensitivity map (η) over the same FOV. The total scan time was approximately 40 min.

MRI data analysis

An open-source software (Elastix, http://elastix.isi.uu.nl/) was used to register the 3D stack of images from all sequences to the first T1 image (TR = 20 ms), to compensate for the potential subject motion between sequences. Potential subject movements during each sequence would result in significant visible artifacts in the images. The scanner operator continuously screened the image quality of each sequence, and those with artifacts were repeated during the same scanning session. All images were smoothed within 3×3 sub-windows using a Gaussian filter before any measurements.

The quantitative MR measurements were performed on a single slice, which was consistently selected by the data analyst in the middle of the tibial shaft. Figure 1B shows schematics of a representative ROI selected manually covering the whole cortical bone region in the tibial midshaft. The average signals within selected ROIs were used to calculate MMF, TWPD, BWPD, PWPD, and MMPD using equations in Appendix I. To investigate the reproducibility of the developed data analysis pipeline, ROIs on bone were selected by 3 independent, experienced readers at the tibial midshaft. For quality control purposes, the ROIs selected by each reader for the first 5 datasets were verified by a board-certified musculoskeletal radiologist. The intraclass correlation coefficient was calculated to compare the T1, MMF, TWPD, BWPD, PWPD, and MMPD in all datasets estimated by the readers.

To investigate the repeatability of the developed UTE-MRI protocol, the lower legs of 3 healthy young volunteers were scanned 3 times at 2-h intervals. Subject positioning, coil setup, and the described sequences were repeated by one operator. In addition to visual comparisons between scans, the average, SD, and coefficient of variation (ie, standard deviation/average) of MMF and proton densities were calculated.

Statistical analysis

One-sample Kolmogorov–Smirnov test was used to determine whether the measured bone proton densities and DXA T-scores in this study were normally distributed. The differences between the 3 participant groups (Young, OPe, and OPo) were examined using the Kruskal–Wallis test by ranks. Spearman's correlation coefficients were calculated between the TH DXA T-score and the MRI-based cortical bone measures. Differences and correlations with P-values below .05 were significant. The post hoc power analysis Student's t-test showed that we have 75% power of detecting a large effect size of 1 (1 standard deviation difference) in comparisons involving the OPe group ($n = 14$), while a large effect size of 0.7 in comparison between OPo and Young groups ($n > 30$). The significance level for multiple comparisons was corrected using the Holm–Bonferroni method. All statistical analyses and image processing steps were performed using MATLAB software (version 2017, The Mathworks Inc.).

Results

The mean age, height, weight, BMI, and TH T-score for each group are presented in Table 1. Age differences between OPo and OPe groups were not significant as examined by the Kruskal–Wallis test by ranks. No significant differences were observed in height, weight, and BMI between groups. The T-score was significantly lower in the OPo than OPe group, as expected based on the study design.

Figure 1 shows representative lower leg axial images (healthy female participant, 25-yr-old) using the UTE and IR-UTE Cones MRI sequences compared with the clinical gradient echo (GRE) sequence. The UTE sequence detected a significant signal in the tibial midshaft cortex, while the GRE sequence resulted in signal voids for both. Compared with the low contrast visualization of bone in UTE-MRI, the IR-UTE MRI sequence visualized cortical bone with high contrast, similar to those contrasts provided by computed tomography. A representative ROI used for MRI analysis is depicted in the UTE image of cortical bone (yellow dashed line).

Figure 2 demonstrates the generated water proton densities (TWPD, BWPD, and PWPD), MMF, and MMPD maps for 3 representative subjects from the Young, OPe, and OPo groups, respectively. For these examples, TWPD and PWPD values were in the following ascending order: Young<OPe < OPo. On the contrary, BWPD, MMF, and MMPD were in the following ascending order: OPo < OPe < Young.

Table 2 presents the average and SD values of UTE-MRI measures performed on the tibial bones of the 3 studied groups. The independent measurements by the readers were averaged to be compared between participant groups. Table 2 also presents the intraclass correlation coefficient (ICC) values between these independent measurements, which were higher than 0.96, indicating a high level of consistency between readers.

The average coefficients of variation for TWPD, BWPD, PWPD, MMF, and MMPD of the tibial bones from 3 repeated acquisitions performed on 3 healthy young volunteers (repeatability study) were 2.3 ± 0.4, 3.0 ± 0.5, 1.9 ± 0.3, 1.0 ± 0.3, and 2.5 ± 0.6% on average, respectively.

Percentage differences and the associated statistical significances ($P < .01$ is significant after correction for multiple comparisons) of all measured MRI biomarkers between the Young, OPe, and OPo groups are presented in Table 3. MMF, BWPD, and MMPD values were significantly lower in OPo patients compared with the young group, while T1, TWPD, and PWPD values were significantly higher in OPo

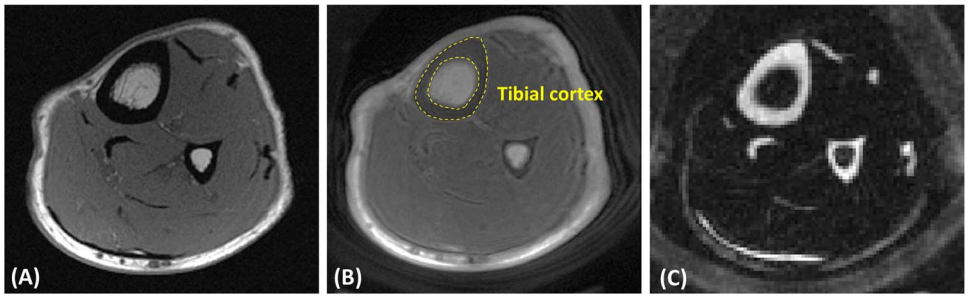

Figure 1. Lower leg MR images in the axial plane of a representative healthy female participant (25 yr old) using (A) a clinical GRE sequence (TE = 8.3 ms and TR = 790 ms), (B) UTE Cones MRI sequence (TE = 0.032 ms and TR = 50 ms), and (C) inversion recovery TE (IR-UTE) (TE = 0.032 ms, TI = 45 ms, and TR = 100 ms). The tibial midshaft cortex is illustrated using a region of interest in the dashed line in Figure 1B.

Table 1. Subjects' characteristics in studied groups.

	Young	OPe	OPo
Number/gender	31/females	14/females	31/females
Age (yr)	28.0 ± 6.1	72.5 ± 6.8	72.0 ± 6.4
Height (m)	1.63 ± 0.11	1.58 ± 0.08	1.63 ± 0.10
Weight (kg)	58.7 ± 11.5	65.0 ± 20.7	58.1 ± 8.9
BMI (kg/m^2)	22.1 ± 3.6	25.6 ± 6.0	22.0 ± 3.8
TH T-Score		−1.90 ± 0.44	−2.59 ± 0.51

Ope, osteopenia; OPo, osteoporosis; TH T-Score, Total Hip DXA T-Score; BMI, Body mass index.

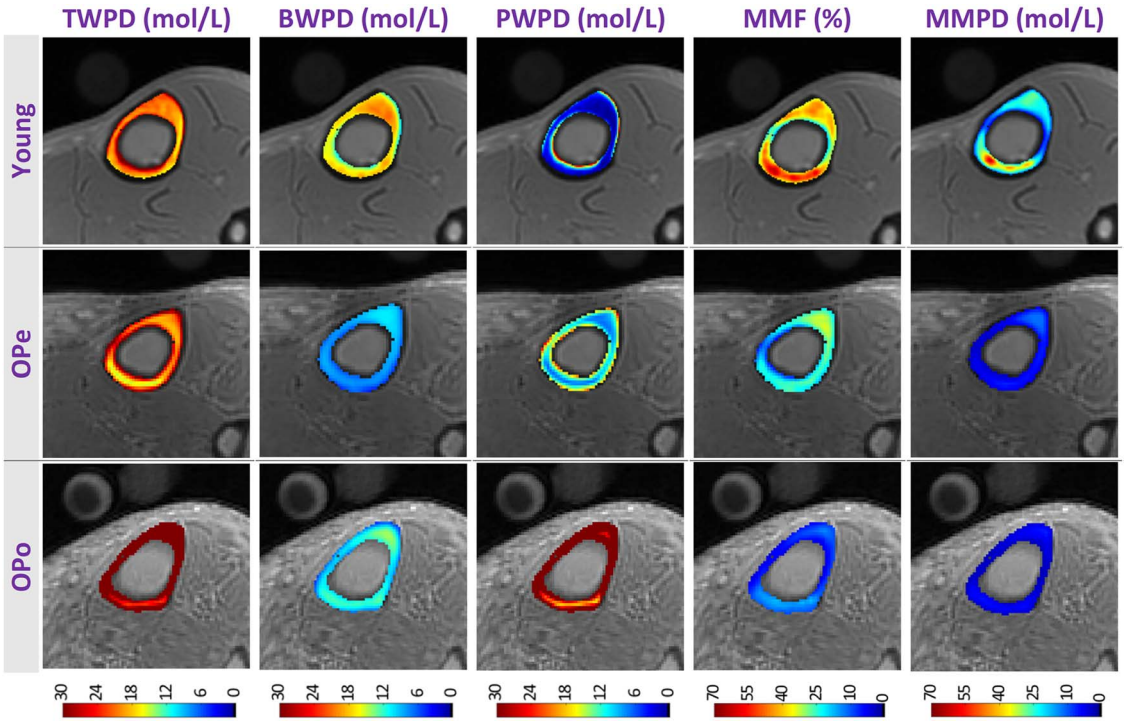

Figure 2. Generated water proton densities (TWPD, BWPD, and PWPD), macromolecular fraction (MMF), and MMPD maps for exemplary participants from the Young group (first row, 35-yr-old female), OPe group (second row, 76-yr-old female), and OPo group (third row, 76-yr-old female). Visual comparison between these examples shows that the TWPD and PWPD were in the following ascending order: Young < OPe < OPo. However, BWPD, MMF, and MMPD were found in the following ascending order: OPo < OPe < Young.

patients compared with the young group. The largest differences between the OPo and Young groups were found in MMF (41.9%), PWPD (103.5%), and MMPD (64.0%) values. PWPD showed significantly higher (50.7%), while BWPD showed significantly lower (16.4%) values in OPe patients vs young subjects. Other UTE-MRI biomarkers showed non-significant differences between the OPe and Young groups. Remarkably, MMF values were found to be significantly lower in OPo patients compared with OPe patients (27% lower in OPo). Other UTE-MRI biomarkers showed non-significant differences between the OPo and OPe groups.

Figure 3 presents the average, median, SD, and first and third quartiles of MMF, TWPD, BWPD, PWPD, MMPD, and T1 values for each group using the whisker's boxplots. Horizontal lines marked with an asterisk indicate the statistically significant differences between groups.

Table 2. Average and SD of UTE-MRI measures for Young, OPe, and OPo groups.

	T1 (ms)	MMF (%)	$T2_{MM}$ (ms)	TWPD (mol/L)	BWPD (mol/L)	PWPD (mol/L)	MMPD (mol/L)
Young	241 ± 21	62 ± 11	15 ± 1	25 ± 3	15 ± 3	10 ± 2	61 ± 42
OPe	262 ± 28	50 ± 10	15 ± 1	27 ± 5	13 ± 1	15 ± 4	35 ± 18
OPo	287 ± 32	36 ± 10	15 ± 1	32 ± 8	11 ± 3	21 ± 7	22 ± 11
ICC	0.96 ± 0.03	0.98 ± 0.01	0.99 ± 0.01	0.97 ± 0.02	0.98 ± 0.01	0.97 ± 0.02	0.96 ± 0.03

BWPD, bound water proton density; MMF, macromolecular fraction; MMPD, macromolecular proton density; Ope, osteopenia; OPo, osteoporosis; PWPD, pore water proton density; TWPD, total water proton density; UTE-MRI, ultrashort echo time magnetic resonance imaging.

Table 3. Percentage differences of UTE-MRI measures between Young, OPe, and OPo groups.

	Percentage difference (%) between cohorts		
	Young-OPe	**Young-OPo**	**OPe-OPo**
T1	8.4 ($P = .10$)	**18.9** ($P < .01$)	9.8 ($P = .08$)
MMF	−20.8 ($P = .04$)	**−41.9** ($P < .01$)	**−27.7** ($P < .01$)
$T2_{MM}$	0.2 ($P = .99$)	1.1 ($P = .23$)	0.5 ($P = .69$)
TWPD	10.5 ($P = .25$)	**25.2** ($P < .01$)	16.7 ($P = .24$)
BWPD	**−16.4** ($P < .01$)	**−27.9** ($P < .01$)	−13.5 ($P = .25$)
PWPD	**50.7** ($P < .01$)	**103.5** ($P < .01$)	41.9 ($P = .04$)
MMPD	−44.4 ($P = .03$)	**−64.0** ($P < .01$)	−37.3 ($P = .06$)

BWPD, bound water proton density; MMF, macromolecular fraction; MMPD, macromolecular proton density; Ope, osteopenia; OPo, osteoporosis; PWPD, pore water proton density; TWPD, total water proton density; UTE-MRI, ultrashort echo time magnetic resonance imaging.

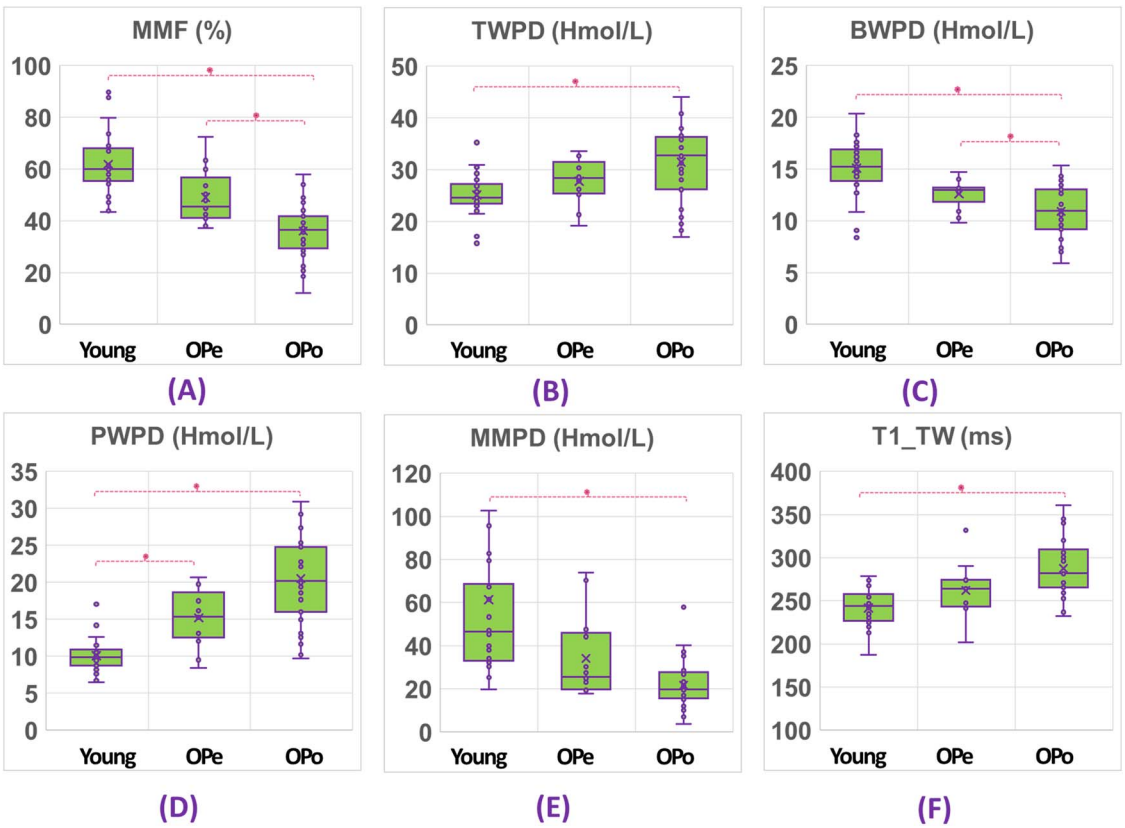

Figure 3. The distribution of the (A) MMF, (B) TWPD, (C) BWPD, (D) PWPD, (E) MMPD, and (F) T1 values in the Young, OPe, and OPo groups shown as Whisker Boxplots Average (marker in the box), median (line in the box), SD (box), and first- and third-quartile values (whiskers) are indicated in the boxplots.

Table 4. Spearman's rank correlation between T-score and UTE-MRI measures.

	T1	MMF	$T2_{MM}$	TWPD	BWPD	PWPD	MMPD
T-score	−0.50 ($P < .01$)	0.56 ($P < .01$)	−0.04 ($P = .77$)	−0.37 ($P < .01$)	0.41 ($P < .01$)	−0.55 ($P < .01$)	0.48 ($P < .01$)
T1	1.00	−0.69 ($P < .01$)	0.04 ($P = .72$)	0.41 ($P < .01$)	−0.53 ($P < .01$)	0.62 ($P < .01$)	−0.44 ($P < .01$)
MMF		1.00	0.01 ($P = .96$)	−0.50 ($P < .01$)	0.54 ($P < .01$)	−0.72 ($P < .01$)	0.82 ($P < .01$)
$T2_{MM}$			1.00	0.14 ($P = .23$)	−0.06 ($P = .59$)	0.16 ($P = .17$)	−0.08 ($P = .48$)
TWPD				1.00	0.14 ($P = .22$)	0.90 ($P < .01$)	−0.24 ($P = .04$)
BWPD					1.00	−0.30 ($P = .01$)	0.43 ($P < .01$)
PWPD						1.00	−0.41 ($P < .01$)
MMPD							1.00

BWPD, bound water proton density; MMF, macromolecular fraction; MMPD, macromolecular proton density; Ope, osteopenia; OPo, osteoporosis; PWPD, pore water proton density; TWPD, total water proton density; UTE-MRI, ultrashort echo time magnetic resonance imaging.

Table 4 presents Spearman's rank correlation coefficients and their significance levels between obtained UTE-MRI measures and TH DXA T-score in postmenopausal participants. T1, MMF, TWPD, PWPD, and MMPD values showed significant correlations with T-scores obtained from DXA scans performed on patients' hips. DXA T-score showed the highest correlations with PWPD ($R = 0.55$) and MMF ($R = 0.56$) values.

UTE-T1 correlation with MMF, BWPD, and PWPD was moderate ($0.53 < R < 0.69$). MMF correlation with T1, TWPD, BWPD, PWPD, and MMPD was moderate to strong ($0.50 < R < 0.82$). TWPD and PWPD correlation was strong ($R = 0.90$). The rest of the correlations were poor or insignificant.

Discussion

This study investigated the differences in water proton densities and macromolecular proton densities between young subjects, OPe patients, and OPo patients. The UTE-MRI-based water and collagen biomarkers investigated in this study significantly differed between OPo patients and young participants. The largest differences between OPo and Young groups were found in MMF, PWPD, and MMPD (Table 3) values. Interestingly, among the measured proton densities, only PWPD was found to be significantly different between the OPe and Young groups. As this increase in pore water content may be the most dominant sign of OPe onset, it is conceivable that PWPD could be used to monitor individuals with bone disease risk.

Remarkably, MMF could distinguish between OPo and OPe patients, with 27% lower values observed in the OPo group. This highlights the potential capability of MMF, a measure of bone collagen content, positioning it as a potential tool for monitoring OPe patients before OPo advancement, or OPo patients undergoing medical interventions. Such MRI-based measures related to bone macromolecular content may become more useful in monitoring patients who undergo unsynchronized mineral and collagen deterioration, such as in osteomalacia,[37,38] which is yet to be investigated in future longitudinal studies. Notably, the relationship between absolute collagen content and the presented UTE-MRI-based measures (MMF and MMPD) still requires further ex vivo validation (eg, Raman spectroscopy and Fourier-transform infrared spectroscopy techniques).

We have investigated the correlations between DXA T-score measured at the hip and proton densities measured at the tibial bone cortex in postmenopausal cohorts. T1, MMF, TWPD, PWPD, and MMPD values showed significant correlations with the T-score. It is likely that bone deterioration takes place across the entire lower extremity at comparable rates, given that UTE-MRI bone assessment of the tibial midshaft correlated significantly with the TH DXA T-score. Remarkably, PWPD and MMF values showed the highest correlations with DXA T-scores, in the range of our recently reported correlations with porosity index and suppression ratio.[24] Although the tibial bone has not been reported as the prominent fracture location in most OPo patients, it is commonly used to study bone fractures as OP is a systematic disease affecting bone at different sites (lower leg, upper leg, wrist, spine, etc.). Since the tibial midshaft has a relatively thick cortex, a robust investigation of the UTE-MRI application has become possible in this study without encountering thin bone with sophisticated morphology in the hip.

The feasibility of in vivo assessment of TWPD, BWPD, PWPD, MMF, and MMPD was investigated in a prior study, where elderly participants demonstrated higher TWPD and PWD values but lower BWPD, MMF, and MMPD values compared with young participants.[32] Although this should be thoroughly investigated in future studies, the MRI-based proton densities estimated in this study are hypothesized to relate to bone microstructural and mechanical properties. Specifically, earlier ex vivo investigations on human cortical bone demonstrated that bone microstructural and mechanical properties were significantly correlated with water proton densities and MMF.[20,21,31-33] Specifically, significant correlations were reported between TWPD in human cortical bone and its μCT-based microstructural properties.[32,39] BWPD has shown significant correlations with the cortical bone mechanical properties,[18,40] though some studies were unable to reproduce this trend.[32] MMF from UTE-MT modeling strongly correlated with human bone microstructural parameters confirmed μCT analysis and histomorphometry,[31,41] and

with mechanical properties.[31-33,41] Notably, the estimated water proton density measures were found to be in the range of previously published values.[23,42,43]

Performing a similar panel of the UTE-MRI sequences on a 1.5 T scanner, which is more ubiquitous in clinics, is feasible after some sequence optimization. Longitudinal relaxation time T1 will be shorter at 1.5 T. The inversion time (TI) needs to be adjusted to null pore water signal for selective imaging of bound water in the cortical bone as we use in the IR-UTE sequence. The signal-to-noise ratio efficiency will be lower at 1.5 T. On the other hand, pore water T2* will be longer at 1.5 Tesla, making it easier to distinguish the bound water with an ultrashort T2* from the pore water with a long T2.

An accurate estimation of water proton densities in bone requires several considerations to be included in the equations, such as the different relaxation times (T1 and T2*) of bone and the external references, the spatial variation in coil sensitivity, in addition to the radiofrequency (RF) pulse duration and its inhomogeneity within the FOV (influencing the actual FA).[44] The T2* term in the proton density measurement could be neglected [Appendix I, eqn. (A1)] as its values were comparable between the external reference phantom and the cortical bone. The T1 effect on the TWPD calculation in PD-weighted 3D UTE sequence could be neglected because of the short $T_{1\text{-}TW}$ of cortical bone, when utilizing a relatively long TR and low FA. However, $T_{1\text{-}TW}$ measurement was performed as the requirement of MT modeling. To ensure an accurate $T_{1\text{-}TW}$ measurement, the B1 inhomogeneity was corrected by considering the actual FA instead of the nominal FA.[36] Assuming a typical uniform IR-UTE signal in cortical bone and using a constant value for $T_{1\text{-}BW}$ from the literature for all subjects ($T_{1\text{-}BW}$ = 135 ms) was practical and accurate for BWPD estimation.[35]

This study was limited in 6 main aspects. First, although the presented MR protocols and techniques were translated to in vivo applications, only a limited number of patients were recruited for this study. The developed techniques need to be examined on a larger group patients, to verify the potential clinical applications in monitoring OPo disease. Second, due to a 40-min scan time, some patients may not be able to remain still for the duration of the scan time. Different MR accelerating techniques have been suggested, such as stretching the readout trajectory, that could be used to accelerate the Cones UTE sequences and reduce the total scan time to nearly 20 min, with negligible resultant errors.[45] Moreover, using a reasonable constant value for T1 while excluding T1 measurement (~20 min of scan time) could be feasible. Future in vivo studies may help generate a T1 selection chart as a function of age, as there is a strong age dependence in T1 relaxation.[46] In situations with limited time and resources, as in clinical cases, calculating PWPD and MMF are the 2 recommended biomarkers that are more discriminatory and show higher correlations with DXA-T-score than other biomarkers. TWPD can replace PWPD, as they were strongly correlated in our results. Third, the presented MR technique in this study did not consider the fat presence impact on cortical bone measures, particularly in regions near the endosteum. It is assumed that the fat signal contribution is likely comparable to PW signal in the UTE images.[47] However, the potential chemical shifts influencing the water and collagen proton densities should be studied in a future investigation. Performing UTE sequences combined with different fat suppression methods, including IDEAL multi-echo acquisition,[48] 2-point or single-point Dixon,[49] and water excitation,[50] could be a feasible path in future studies. Fourth, the diagnosis of diabetes, renal, thyroid, and parathyroid diseases, history of fracture, smoking, alcohol consumption, or current medication, all of which may influence bone health, have not been recorded for the included patients in this study. Future investigations should consider controlling such important factors between studied groups. Fifth, the measurements in this study were performed on a single slice in the middle of scanning coverage (middle of the tibial shaft), which was consistently selected by an experienced operator. However, potential bone variations along the tibia likely influenced the presented results in this study. ROI selection through all image slices, potentially using an automatic approach may help to investigate the variations of the proposed MRI measures across the entire scanned volumes. Future investigations should also focus on the potential size dependency in the quantitative MRI measure presented in this study that may be influenced by the size of the bone in subjects and the selected ROIs. Sixth, DXA scans and analyses were not performed by the investigators to confirm their accuracy. The provided DXA reports by patients were from 3 different medical facilities, the scanners were different, and the recorded information was incomplete for all reports. Therefore, only the TH T-score was used in this study, which was common in all patients' documents and could be trusted regardless of the differences in the methods. Future investigations should ensure rigorous study design for both MRI and DXA analyses.

Conclusion

We investigated the differences in water and macromolecular contents measured with UTE-MRI in tibial cortical bone, between female post-menopausal OPe and OPo patients and young participants. MMF, BWPD, and MMPD were significantly lower in OPo patients compared with the young group, whereas T1, TWPD, and PWPD were significantly higher in OPo patients. The largest OPo/Young average percentage differences were found in MMF, PWPD, and MMPD. PWPD was significantly higher, while BWPD was significantly lower in OPe than in the Young group. Remarkably, MMF was significantly lower in OPo vs OPe group. MMF and PWPD showed significant correlations with the DXA-T score. Therefore, they were recommended to evaluate individuals with OPe and OPo.

Author contributions

Saeed Jerban (Conceptualization, Data curation, Formal analysis, Investigation, Methodology, Validation, Visualization, Writing—original draft, Writing—review & editing [equal]), Yajun Ma (Conceptualization, Data curation, Formal analysis, Investigation, Methodology, Software, Writing—review & editing [equal]), Zhao Wei (Data curation, Formal analysis, Methodology, Writing—review & editing), Meghan Shen(Formal analysis, Methodology, Writing—review & editing), Zubaid Ibrahim (Formal analysis, Methodology, Writing—review & editing), Hyungseok Jang (Investigation, Methodology), Pengzhe Lu (Conceptualization, Investigation, Writing—review & editing), Douglas G. Chang (Conceptualization, Investigation, Methodology, Writing—review & editing), Gina Woods (Conceptualization, Investigation, Methodology, Writing—review & editing), Christine B. Chung (Conceptualization, Investigation, Supervision, Writing—review & editing), Eric Y. Chang (Conceptualization, Funding acquisition, Methodology, Supervision, Writing—review &

editing), and Jiang Du (Conceptualization, Investigation, Methodology, Resources, Supervision, Writing—original draft, Writing—review & editing)

Funding

We acknowledge the grant support from the National Institutes of Health (K01AR080257, R01AR068987, R01AR062581, R01AR075825, R01AR079484, R01AR07887, and 5P30AR073761), Veterans Affairs Clinical Science and Rehabilitation Research and Development (I01CX001388, I01RX002604, and I01CX000625), and GE Healthcare.

Conflicts of interest

The authors have no conflicts of interest to declare.

Data availability

The data and analytic code for this study may be made available from the corresponding author upon reasonable request.

References

1. Zanker J, Duque G. Osteoporosis in older persons: old and new players. *J Am Geriatr Soc*. 2019;67(4):831–840. https://doi.org/10.1111/jgs.15716
2. Guerri S, Mercatelli D, Gómez MPA, et al. Quantitative imaging techniques for the assessment of osteoporosis and sarcopenia. *Quant Imaging Med Surg*. 2018;8(1):60–85. https://doi.org/10.21037/qims.2018.01.05
3. Looker AC, Frenk SM. Percentage of adults aged 65 and over with osteoporosis or low bone mass at the femur neck or lumbar spine: United States, 2005–2010. Centers for Disease Control and Prevention. 2015;2005–2010.
4. Dimai HP. Use of dual-energy X-ray absorptiometry (DXA) for diagnosis and fracture risk assessment; WHO-criteria, T- and Z-score, and reference databases. *Bone*. 2017;104(11):39–43. https://doi.org/10.1016/j.bone.2016.12.016
5. Wáng YXJ, Griffith JF, Blake GM, et al. Revision of the 1994 World Health Organization T-score definition of osteoporosis for use in older East Asian women and men to reconcile it with their lifetime risk of fragility fracture. *Skeletal Radiol*. 2023;53(4):609–625. https://doi.org/10.1007/s00256-023-04481-7
6. Noel SE, Santos MP, Wright NC. Racial and ethnic disparities in bone health and outcomes in the United States. *J Bone Miner Res*. 2021;36(10):1881–1905. https://doi.org/10.1002/jbmr.4417
7. MacDonald HM, Nishiyama KK, Kang J, Hanley DA, Boyd SK. Age-related patterns of trabecular and cortical bone loss differ between sexes and skeletal sites: a population-based HR-pQCT study. *J Bone Miner Res*. 2011;26(1):50–62. https://doi.org/10.1002/jbmr.171
8. Lees S. A mixed packing model for bone collagen. *Calcif Tissue Int*. 1981;33(1):591–602. https://doi.org/10.1007/BF02409497
9. Burr DB. The contribution of the organic matrix to bone's material properties. *Bone*. 2002;31(1):8–11. https://doi.org/10.1016/S8756-3282(02)00815-3
10. Trajanoska K, Schoufour JD, de Jonge EAL, et al. Fracture incidence and secular trends between 1989 and 2013 in a population based cohort: the Rotterdam Study. *Bone*. 2018;114(September):116–124. https://doi.org/10.1016/j.bone.2018.06.004
11. Chang EY, Du J, Chung CB. UTE imaging in the musculoskeletal system. *J Magn Reson Imaging*. 2015;41(4):870–883.
12. Du J, Bydder GM. Qualitative and quantitative ultrashort-TE MRI of cortical bone. *NMR Biomed*. 2013;26(5):489–506.
13. Chang EY, Du J, Bae WC, Statum S, Chung CB. Effects of Achilles tendon immersion in saline and perfluorochemicals on T2 and T2*. *J Magn Reson Imaging*. 2014;40(2):496–500. https://doi.org/10.1002/jmri.24360
14. Rajapakse CS, Bashoor-Zadeh M, Li C, Sun W, Wright AC, Wehrli FW. Volumetric cortical bone porosity assessment with MR imaging: validation and clinical feasibility. *Radiology*. 2015;276(2):526–535.
15. Seifert AC, Wehrli FW. Solid-state quantitative 1H and 31P MRI of cortical bone in humans. *Curr Osteoporos Rep*. 2016;14(3):77–86. https://doi.org/10.1007/s11914-016-0307-2
16. Nyman JS, Ni Q, Nicolella DP, Wang X. Measurements of mobile and bound water by nuclear magnetic resonance correlate with mechanical properties of bone. *Bone*. 2008;42(1):193–199. https://doi.org/10.1016/j.bone.2007.09.049
17. Du J, Hermida JC, Diaz E, et al. Assessment of cortical bone with clinical and ultrashort echo time sequences. *Magn Reson Med*. 2013;70(3):697–704. https://doi.org/10.1002/mrm.24497
18. Manhard MK, Uppuganti S, Granke M, Gochberg DF, Nyman JS, Does MD. MRI-derived bound and pore water concentrations as predictors of fracture resistance. *Bone*. 2016;87(6):1–10.
19. Jerban S, Chang DG, Ma Y, Jang H, Chang EY, Du J. An update in qualitative imaging of bone using ultrashort Echo time magnetic resonance. *Front Endocrinol*. 2020;11(1):677–689. https://doi.org/10.3389/fendo.2020.555756
20. Ma Y-J, Jerban S, Jang H, Chang D, Chang EY, Du J. Quantitative ultrashort Echo time (UTE) magnetic resonance imaging of bone: an update. *Front Endocrinol*. 2020;11(1):667–676.
21. Jerban S, Ma Y, Wei Z, Jang H, Chang EY, Du J. Quantitative magnetic resonance imaging of cortical and trabecular bone. *Semin Musculoskelet Radiol*. 2020;24(4):386–401. https://doi.org/10.1055/s-0040-1710355
22. Jones BC, Wehrli FW, Kamona N, et al. Automated, calibration-free quantification of cortical bone porosity and geometry in postmenopausal osteoporosis from ultrashort echo time MRI and deep learning. *Bone*. 2023;171(6):116743. https://doi.org/10.1016/j.bone.2023.116743
23. Jones BC, Lee H, Cheng C-C, et al. MRI quantification of cortical bone porosity, mineralization, and morphologic structure in postmenopausal osteoporosis. *Radiology*. 2023;307(2):e221810. https://doi.org/10.1148/radiol.221810
24. Jerban S, Ma Y, Moazamian D, et al. MRI-based porosity index (PI) and suppression ratio (SR) in the tibial cortex show significant differences between normal, osteopenic, and osteoporotic female subjects. *Front Endocrinol*. 2023;14:1148345. https://doi.org/10.3389/fendo.2023.1148345
25. Jerban S, Ma Y, Alenezi S, et al. Ultrashort Echo time (UTE) MRI porosity index (PI) and suppression ratio (SR) correlate with the cortical bone microstructural and mechanical properties: ex vivo study. *Bone*. 2023;169(4):116676. https://doi.org/10.1016/j.bone.2023.116676
26. Jerban S, Ma Y, Namiranian B, et al. Age-related decrease in collagen proton fraction in tibial tendons estimated by magnetization transfer modeling of ultrashort echo time magnetic resonance imaging (UTE-MRI). *Sci Rep*. 2019;9(1):17974. https://doi.org/10.1038/s41598-019-54559-3
27. Jerban S, Ma Y, Afsahi AM, et al. Lower macromolecular content in tendons of female patients with osteoporosis versus patients with osteopenia detected by ultrashort Echo time (UTE) MRI. *Diagnostics*. 2022;12(5):1061.
28. Du J, Chiang AJT, Chung CB, et al. Orientational analysis of the Achilles tendon and enthesis using an ultrashort echo time spectroscopic imaging sequence. *Magn Reson Imaging*. 2010;28(2):178–184.
29. Ma Y, Chang EY, Carl M, Du J. Quantitative magnetization transfer ultrashort echo time imaging using a time-efficient 3D multispoke cones sequence. *Magn Reson Med*. 2017;79(2):692–700. https://doi.org/10.1002/mrm.26716
30. Ma Y, Shao H, Du J, Chang EY. Ultrashort echo time magnetization transfer (UTE-MT) imaging and modeling: magic angle independent biomarkers of tissue properties. *NMR Biomed*. 2016;29(11):1546–1552. https://doi.org/10.1002/nbm.3609
31. Jerban S, Ma Y, Wong J, et al. Ultrashort echo time magnetic resonance imaging (UTE-MRI) of cortical bone correlates

well with histomorphometric assessment of bone microstructure. *Bone*. 2019;123(123):8–17. https://linkinghub.elsevier.com/retrieve/pii/S8756328219300894. https://doi.org/10.1016/j.bone.2019.03.013
32. Jerban S, Ma Y, Li L, et al. Volumetric mapping of bound and pore water as well as collagen protons in cortical bone using 3D ultrashort Echo time cones MR imaging techniques. *Bone*. 2019;127(10):120–128. https://linkinghub.elsevier.com/retrieve/pii/S8756328219302224. https://doi.org/10.1016/j.bone.2019.05.038
33. Jerban S, Ma Y, Dorthe EW, et al. Assessing cortical bone mechanical properties using collagen proton fraction from ultrashort echo time magnetization transfer (UTE-MT) MRI modeling. *Bone Rep*. 2019;11(2):100220. https://linkinghub.elsevier.com/retrieve/pii/S2352187219300269. https://doi.org/10.1016/j.bonr.2019.100220
34. Ma Y, Tadros A, Du J, Chang EY. Quantitative two-dimensional ultrashort echo time magnetization transfer (2D UTE-MT) imaging of cortical bone. *Magn Reson Med*. 2018;79(4):1941–1949. https://doi.org/10.1002/mrm.26846
35. Chen J, Chang EY, Carl M, et al. Measurement of bound and pore water T1 relaxation times in cortical bone using three-dimensional ultrashort echo time cones sequences. *Magn Reson Med*. 2016;77(6):2136–2145.
36. Ma Y, Lu X, Carl M, et al. Accurate T 1 mapping of short T 2 tissues using a three-dimensional ultrashort echo time cones actual flip angle imaging-variable repetition time (3D UTE-cones AFI-VTR) method. *Magn Reson Med*. 2018;80(2):598–608. https://doi.org/10.1002/mrm.27066
37. Anumula S, Magland J, Wehrli SL, Ong H, Song HK, Wehrli FW. Multi-modality study of the compositional and mechanical implications of hypomineralization in a rabbit model of osteomalacia. *Bone*. 2008;42(2):405–413. https://doi.org/10.1016/j.bone.2007.10.011
38. Becker C. 28 - Osteomalacia. In: Kleerekoper M, Siris ES, McClung MB, The Bone and Mineral Manual (Second Edition), A Practical Guide (Second EMM, editors. Burlington: Academic Press; 2005:141–146. http://www.sciencedirect.com/science/article/pii/B9780120885695500292
39. Jerban S, Ma Y, Jang H, et al. Water proton density in human cortical bone obtained from ultrashort echo time (UTE) MRI predicts bone microstructural properties. *Magn Reson Imaging*. 2020;67(1):85–89. https://doi.org/10.1016/j.mri.2020.01.004
40. Horch RA, Gochberg DF, Nyman JS, Does MD. Clinically compatible MRI strategies for discriminating bound and pore water in cortical bone. *Magn Reson Med*. 2012;68(6):1774–1784. https://doi.org/10.1002/mrm.24186
41. Jerban S, Ma Y, Wan L, et al. Collagen proton fraction from ultrashort echo time magnetization transfer (UTE-MT) MRI modelling correlates significantly with cortical bone porosity measured with micro-computed tomography (μCT). *NMR Biomed*. 2019;32(2):e4045.
42. Zhao X, Song HK, Seifert AC, Li C, Wehrli FW. Feasibility of assessing bone matrix and mineral properties in vivo by combined solidstate 1H and 31P MRI. *PLoS One*. 2017;12(3):1–16. https://doi.org/10.1371/journal.pone.0173995
43. Manhard MK, Horch RA, Gochberg DF, Nyman JS, Does MD. In vivo quantitative MR imaging of bound and pore water in cortical bone. *Radiology*. 2015;277(1):221–229. https://doi.org/10.1148/radiol.2015140336
44. Du J, Carl M, Bydder M, Takahashi A, Chung CB, Bydder GM. Qualitative and quantitative ultrashort echo time (UTE) imaging of cortical bone. *J Magn Reson*. 2010;207(2):304–311.
45. Wan L, Zhao W, Ma Y, et al. Fast quantitative three-dimensional ultrashort echo time (UTE) magnetic resonance imaging of cortical bone using extended cones sampling. *Magn Reson Med*. 2019;82(1):225–236. https://doi.org/10.1002/mrm.27715
46. Reichert ILH, Robson MD, Gatehouse PD, et al. Magnetic resonance imaging of cortical bone with ultrashort TE pulse sequences. *Magn Reson Imaging*. 2005;23(5):611–618.
47. Lu X, Jerban S, Wan L, et al. Three dimensional ultrashort echo time imaging with tri-component analysis for human cortical bone. *Magn Reson Med*. 2019;82(1):348–355. https://doi.org/10.1002/mrm.27718
48. Gee CS, Nguyen JTK, Marquez CJ, et al. Validation of bone marrow fat quantification in the presence of trabecular bone using MRI. *J Magn Reson Imaging*. 2015;42(2):539–544. https://doi.org/10.1002/jmri.24795
49. Jang H, Carl M, Ma Y, et al. Fat suppression for ultrashort echo time imaging using a single point dixon method. *NMR Biomed*. 2019;32(5):e4069. https://doi.org/10.1002/nbm.4069
50. Ma Y-J, Jerban S, Jang H, Chang EY, Du J. Fat suppression for ultrashort echo time imaging using a novel soft-hard composite radiofrequency pulse. *Magn Reson Med*. 2019;82(6):2178–2187. https://doi.org/10.1002/mrm.27885
51. Manhard MK, Harkins KD, Gochberg DF, Nyman JS, Does MD. 30-Second bound and pore water concentration mapping of cortical bone using 2D UTE with optimized half-pulses. *Magn Reson Med*. 2017;77(3):945–950. https://doi.org/10.1002/mrm.26605
52. Ma YJ, Zhu Y, Lu X, Carl M, Chang EY, Du J. Short T 2 imaging using a 3D double adiabatic inversion recovery prepared ultrashort echo time cones (3D DIR-UTE-cones) sequence. *Magn Reson Med*. 2017;79(5):1–9.

Appendix I

Estimating the TWPD

Comparing the UTE MRI signal of bone with the external reference signal can provide an estimation of the TWPD in the cortex.[12,15,28,42,43,51] Ernst equation can be used to predict the UTE-MRI [eqn. (A.1)].[44]

$$SI_{Bone}\,(\mathrm{TE}) \propto \frac{1-e^{-TR/T_{1-TW}}}{1-\cos\theta \times e^{-TR/T_{1-TW}}} \times e^{-TE/T^{*}_{2-TW}} \times TWPD, \quad (A.1)$$

where θ, TR, and $T_{1\text{-}TW}$ are flip angle (FA), repetition time, and the spin–lattice relaxation time of total water, respectively. By acquiring a PD-weighted UTE MRI, we can simplify the equation while avoiding significant potential errors. This can be achieved by using an ultrashort TE of 32 μs, a relatively long TR equal to 50 ms, and a low FA equal to 10°. Moreover, as mentioned in the Discussion section, the T1 and T2* effects can be neglected because the excitation pulse duration is very short and the $T2^{*}_{REF}$ and $T2^{*}_{TW}$ are much longer than the TE in this study. As a result, eqn. (A2) can be used to estimate TWPD by comparing the UTE signals of the external reference and the cortical bone.

$$TWPD \approx \frac{SI^{UTE}_{Bone}}{SI^{UTE}_{REF}} \times \eta \times \rho_{\mathrm{REF}}, \quad (A.2)$$

where ρ_{REF} and η and are the proton density of the external reference and the coil sensitivity, respectively.

Estimating the BWPD

Comparing the IR-UTE MRI signal of bone with the external reference signal can provide an estimation of the BWPD in the cortex.[12,15,28,42,43,51] Equation (A.3) can be used to predict the IR-UTE signal approximately if a complete saturation of BW signal can be assumed (ie, an efficient pore water nulling).[44] Therefore, eqn. (A.4) can be used to estimate BWPD, which compares the IR-UTE signals of the external reference and the cortical bone ($T2^*_{BW} \approx 350\ \mu s$, $T2^*_{REF} \approx 350\ \mu s$, $T_{1\text{-}REF} \approx 6$ ms, and TE = 32 μs).

$$SI(t)_{IR-UTE} \propto \left(e^{-TI/T_{1-BW}}\right) \times \sin\theta \times e^{-TE/T_2^*} \times BWPD \tag{A.3}$$

$$BWPD \approx \frac{SI_{Bone}^{IR-UTE}}{SI_{REF}^{IR-UTE}} \times \eta \times \rho_{REF} \times \frac{1}{1-e^{-TI/T_{1-BW}}}, \tag{A.4}$$

where $T_{1\text{-}BW}$ refers to the T1 of BW.

Estimating the PWPD

As presented in eqn. (A.5), subtracting BWPD from TWPD results in PWPD estimation.

$$PWPD = TWPD - BWPD \tag{A.5}$$

Estimating the MMPD

The estimated TWPD in eqn. (A.2) combined with the MMF measured from the 2-pool MT modeling can be used to calculate MMPD.[30,52] MMF is the macromolecular proton fraction, an output from MT modeling, which is defined as the ratio between MMPD and TWPD (TWPD+MMPD). Thus, eqn. (A.6) can be used to calculate MMPD.

$$MMPD = \frac{TWPD \times MMF}{1 - MMF} \tag{A.6}$$